15 P

Analysis of a Disk-on-Rod Surface Wave Element Inside a Corrugated Horn Using the Mode-Matching Technique

J. C. Chen
Ground Antennas and Facilities Engineering Section

A disk-on-rod inside a corrugated horn is one of the horn configurations for dual-frequency or wide-band operation. A mode-matching analysis method is described. A disk-on-rod inside a corrugated horn is represented as a series of coaxial waveguide sections and circular waveguide sections connected to each other. Three kinds of junctions need to be considered: coaxial-to-coaxial, coaxial-to-circular, and circular-to-circular. A computer program was developed to calculate the scattering matrix and the radiation pattern of a disk-on-rod inside a corrugated horn. The software was verified by experiment, and good agreement between calculation and measurement was obtained. The disk-on-rod inside a corrugated horn design gives an option to the Deep Space Network dual-frequency operation system, which currently is a two-horn/one-dichroic plate system.

I. Introduction

To design a dual-frequency horn for the DSS-13 beam waveguide antenna, an analysis tool needs to be developed. A side-view model of a circularly symmetric disk-on-rod inside a corrugated horn is shown in Fig. 1. The horn is subdivided to several sections that are either coaxial or circular waveguide sections. The junctions between these sections are either coaxial-to-coaxial, coaxial-to-circular, or circular-to-circular waveguide junctions. In order to analyze the performance of a disk-on-rod inside a corrugated horn, a computer program based on the mode-matching method was developed [1,2]. The circular waveguide program and coaxial waveguide program that calculate the scattering matrix of the circular waveguide and coaxial waveguide of different sizes, respectively, are already available [3]. In order to simulate the disk-on-rod inside a corrugated horn, it was necessary to integrate the existing circular waveguide program and coaxial program with a new third program that handles the junction between circular and coaxial waveguides.

II. Theory

The analysis of the waveguide junctions is based on the mode-matching method. The following theory is used to calculate the scattering matrix of coaxial-to-circular waveguide junctions (Fig. 2). The electromagnetic field is represented by coaxial waveguide modes in the coaxial waveguide region and circular waveguide modes in the circular waveguide region. Only waveguide modes of order 1 are considered in
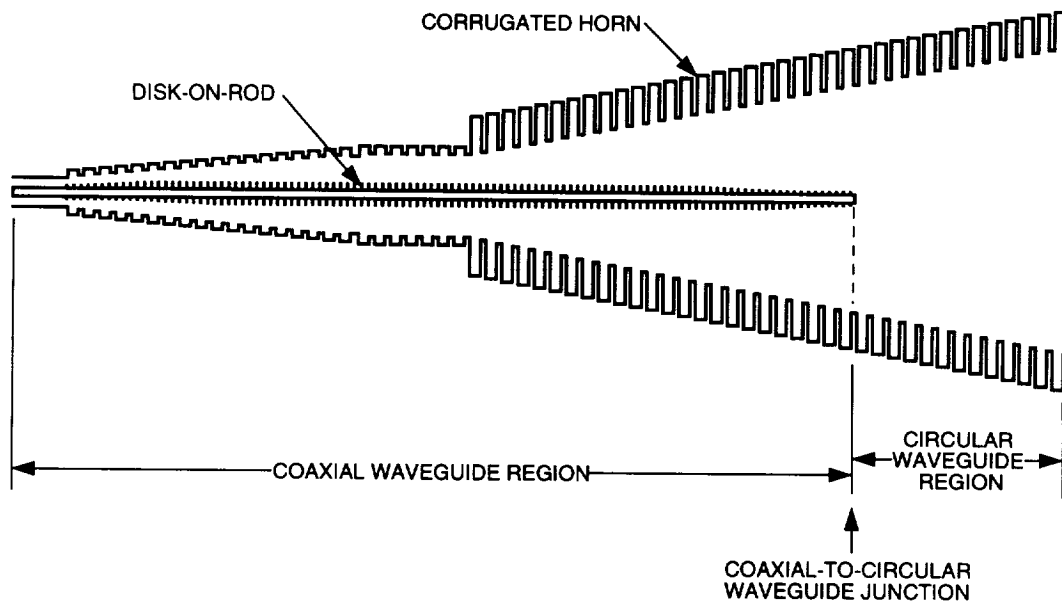
CORRUGATED HORN

DISK-ON-ROD

COAXIAL WAVEGUIDE REGION

CIRCULAR WAVEGUIDE REGION

COAXIAL-TO-CIRCULAR WAVEGUIDE JUNCTION

Fig. 1. A model of a disk-on-rod inside a corrugated horn.

(a)

REGION I
M MODES

REGION II
N MODES

A_I

A_{II}

a_I
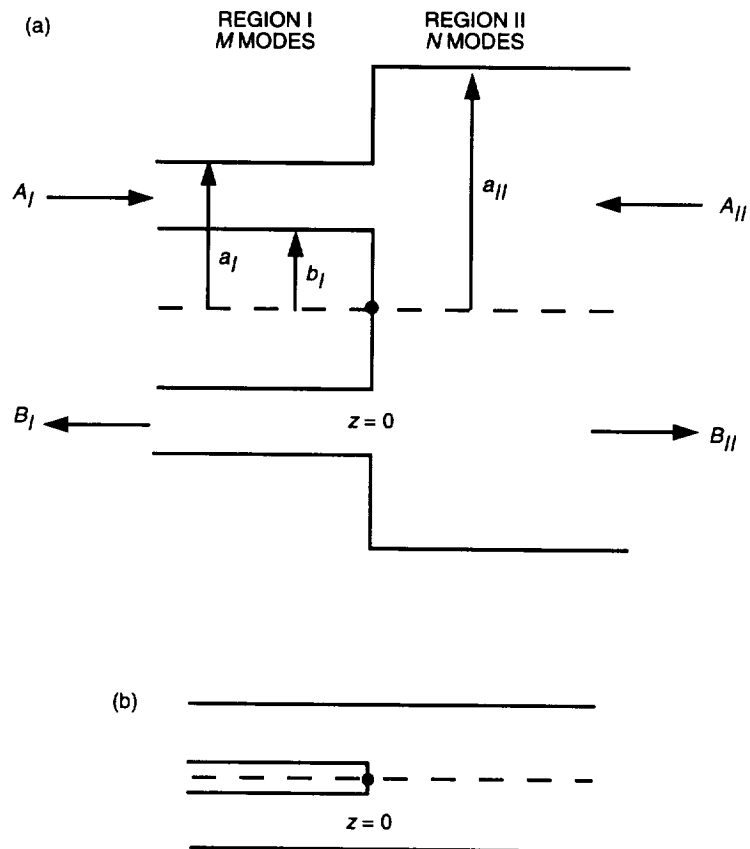
b_I

a_{II}

B_I

$z = 0$

B_{II}

(b)

$z = 0$

Fig. 2. Coaxial-to-circular waveguide junctions with (a) a different outer radius and (b) the same outer radius.

the analysis, and the waveguide is assumed to be nondissipative. In region I (the coaxial waveguide region), let the transverse field $\overline{E}_I, \overline{H}_I$ at $z = 0$ be represented by the modal expansion

$$\overline{E}_I = \sum_{m=1}^{M} (A_{mI} + B_{mI}) \overline{e}_{mI} \tag{1}$$

$$\overline{H}_I = \sum_{m=1}^{M} (A_{mI} - B_{mI}) \overline{h}_{mI} \tag{2}$$

where $\overline{e}_{mI}$ and $\overline{h}_{mI}$ are transverse modal field vectors and A_{mI}, B_{mI} are the forward and reflected modal coefficients in the region I to be determined. The electromagnetic fields for the TE ($e_z = 0$) and TM ($h_z = 0$) coaxial modes are as follows [4].

For the TE coaxial waveguide modes, the transverse $\overline{e}$ and $\overline{h}$ fields are

$$\overline{e} = e_r \hat{r} + e_\phi \hat{\phi} \tag{3}$$

$$\overline{h} = h_r \hat{r} + h_\phi \hat{\phi} \tag{4}$$

$$e_r = C_m \frac{F_1 \left((\chi'_m r)/b_I \right)}{(\chi'_m r)/b_I} \sin \phi$$

$$e_\phi = C_m F_1' \left(\frac{\chi'_m r}{b_I} \right) \cos \phi \tag{5}$$

$$h_r = -\frac{e_\phi}{\eta_m^{TE}}$$

$$h_\phi = \frac{e_r}{\eta_m^{TE}} \tag{6}$$

where F_1 is a combination of Bessel functions of the first kind, $J_\nu(z)$, and Bessel functions of the second kind, $Y_\nu(z)$, of integral order $\nu = 1$, and is given by

$$F_1 \left(\frac{\chi'_m r}{b_I} \right) = J_1 \left(\frac{\chi'_m r}{b_I} \right) Y_1'(\chi'_m) - Y_1 \left(\frac{\chi'_m r}{b_I} \right) J_1'(\chi'_m) \tag{7}$$

where χ'_m is the mth root of the derivative of F_1 when $r = a_I$ and C_m is a normalization constant. The impedance of the TE waveguide mode, η^{TE}, is given by

$$\eta^{TE} = \begin{cases} \dfrac{\sqrt{\mu/\varepsilon}}{\sqrt{1 - (\lambda/\lambda_c)^2}} & \text{for } \lambda < \lambda_c \\[3mm] \dfrac{j\sqrt{\mu/\varepsilon}}{\sqrt{(\lambda/\lambda_c)^2 - 1}} & \text{for } \lambda > \lambda_c \end{cases} \tag{8}$$

where μ and ε are the absolute magnetic permeability and absolute dielectric constant of the medium, respectively. The free space wavelength is λ, and λ_c is the cutoff wavelength ($\lambda_c = \lambda'_{cm}$) of the TE coaxial waveguide mode, which can be expressed as

$$\lambda'_{cm} = \frac{2\pi}{((a_I/b_I) + 1)\chi'_m}(a_I + b_I) \qquad m = 1$$

$$\lambda'_{cm} = \frac{2\pi}{((a_I/b_I) - 1)\chi'_m}(a_I - b_I) \qquad m = 2, 3, 4, \cdots$$

(9)

For the TM coaxial waveguide modes, the transverse $\bar{e}$ and $\bar{h}$ fields can be expressed as

$$e_r = -C_m G_1' \left(\frac{\chi_m r}{b_I}\right) \cos\phi$$

$$e_\phi = C_m \frac{G_1 \left(\chi_m r/b_I\right)}{\chi_m r/b_I} \sin\phi$$

(10)

$$h_r = -\frac{e_\phi}{\eta_m^{TM}}$$

$$h_\phi = \frac{e_r}{\eta_m^{TM}}$$

(11)

where G_1 is a combination of Bessel functions of the first kind, $J_\nu(x)$, and Bessel functions of the second kind, $Y_\nu(x)$, of integral order $\nu = 1$, and is given by

$$G_1 \left(\frac{\chi_m r}{b_I}\right) = J_1 \left(\frac{\chi_m r}{b_I}\right) Y_1(\chi_m) - Y_1 \left(\frac{\chi_m r}{b_I}\right) J_1(\chi_m)$$

(12)

where χ_m is the mth root of G_1 when $r = a_I$. The impedance of the TM waveguide mode, η^{TM}, is

$$\eta^{TM} = \begin{cases} \sqrt{\frac{\mu}{\varepsilon}}\sqrt{1 - \left(\frac{\lambda}{\lambda_c}\right)^2} & \text{for } \lambda < \lambda_c \\ -j\sqrt{\frac{\mu}{\varepsilon}}\sqrt{\left(\frac{\lambda}{\lambda_c}\right)^2 - 1} & \text{for } \lambda > \lambda_c \end{cases}$$

(13)

The cutoff wavelength of the TM coaxial waveguide mode, $\lambda_c = \lambda_{cm}$, can be expressed as

$$\lambda_{cm} = \frac{2\pi}{((a_I/b_I) - 1)\chi_m}(a_I - b_I)$$

(14)

In region II, the transverse fields $\overline{E}_{II}, \overline{H}_{II}$ at $z = 0$ can be represented by the modal solution in region II (the circular waveguide region) as follows:

$$\overline{E}_{II} = \sum_{n=1}^{N}(A_{nII} + B_{nII})\overline{e}_{nII} \tag{15}$$

$$\overline{H}_{II} = \sum_{n=1}^{N}(A_{nII} - B_{nII})\overline{h}_{nII} \tag{16}$$

where $\overline{e}_{nII}$ and $\overline{h}_{nII}$ are transverse modal fields and A_{nII}, B_{nII} are the forward and reflected modal coefficients in region II to be determined.

The transverse $\overline{e}$ and $\overline{h}$ fields of the TE circular waveguide modes are

$$e_r = C_n \frac{J_1((\chi_n'r)/a_{II})}{(\chi_n'r)/a_{II}} \sin\phi$$

$$e_\phi = C_n J_1'\left(\frac{\chi_n'r}{a_{II}}\right)\cos\phi \tag{17}$$

$$h_r = -\frac{e_\phi}{\eta_n^{TE}}$$

$$h_\phi = \frac{e_r}{\eta_n^{TE}} \tag{18}$$

where χ_n' is the nth nonvanishing root of the derivative of the Bessel function $J_1'(\chi_n') = 0$. The C_n is a normalization constant. The impedance of the TE waveguide mode, η^{TE}, is defined in Eq. (6), and the cutoff wavelength of the TE circular waveguide mode, $\lambda_c = \lambda_{cn}'$, can be expressed as

$$\lambda_{cn}' = \frac{2\pi}{\chi_n'}a_{II} \tag{19}$$

For TM circular waveguide modes, the transverse $\overline{e}$ and $\overline{h}$ fields are

$$e_r = -C_n J_1'\left(\frac{\chi_n r}{a_{II}}\right)\cos\phi$$

$$e_\phi = C_n \frac{J_1((\chi_n r)/a_{II})}{(\chi_n r)/a_{II}} \sin\phi \tag{20}$$

$$h_r = -\frac{e_\phi}{\eta_n^{TM}}$$

$$h_\phi = \frac{e_r}{\eta_n^{TM}} \tag{21}$$

192

and χ_n is the nth nonvanishing root of $J_1(\chi_n) = 0$. The impedance of the TM waveguide mode, η^{TM}, is defined in Eq. (11), and the cutoff wavelength, $\lambda_c = \lambda_{cn}$, of the TM circular waveguide mode can be expressed as

$$\lambda_{cn} = \frac{2\pi}{\chi_n} a_{II} \tag{22}$$

By applying the boundary conditions that are discussed in detail in [1], the following pair of simultaneous matrix equations is obtained:

$$[P]\{[A_I] + [B_I]\} = [Q]\{[A_{II}] + [B_{II}]\} \tag{23}$$

$$[P]^T\{[B_{II}] - [A_{II}]\} = [R]\{[A_I] - [B_I]\} \tag{24}$$

where $[A_I]$ and $[B_I]$ are column matrices of M elements containing the unknown modal coefficients in region I; $[A_{II}]$ and $[B_{II}]$ are column matrices of N elements containing the unknown modal coefficients in region II; $[P]^T$ is a transpose matrix of $[P]$; $[P]$ is an M-by-N matrix; $[Q]$ is an N-by-N diagonal matrix; and $[R]$ is an M-by-M diagonal matrix. The elements of these three matrices, $[P], [Q]$, and $[R]$, are defined as follows:

$$P_{mn} = \int_{S_I} \underline{e}_{mI} \times \underline{h}_{nII} \cdot ds \tag{25}$$

$$Q_{nn} = \int_{S_{II}} \underline{e}_{nII} \times \underline{h}_{nII} \cdot ds \tag{26}$$

$$R_{mm} = \int_{S_I} \underline{e}_{mI} \times \underline{h}_{mI} \cdot ds \tag{27}$$

In all cases, these integrals can be obtained in closed form. The R_{mm} is the integration between two circular waveguide modes and Q_{nn} is the integration between two coaxial waveguide modes in region I and region II, respectively; P_{mn} is the integration between circular and coaxial waveguide modes and can be expressed as

$$P_{mn} = \begin{cases} \left(\frac{\pi}{\eta_n^{TE}} C_n C_m\right) \frac{1}{(\chi'_n/a_{II})^2 - (\chi'_m/b_I)^2} \left[\frac{2}{\pi} J'_1\left(\frac{\chi'_n b_I}{a_{II}}\right) - \frac{\chi'_m a_I}{b_I} J'_1\left(\frac{\chi'_n a_I}{a_{II}}\right) F_1\left(\frac{\chi'_m a_I}{b_I}\right)\right] \\ \quad \text{(TE coaxial waveguide mode and TE circular waveguide mode)} \\[1em] \left(\frac{\pi}{\eta_n^{TM}} C_n C_m\right) \frac{1}{(\chi_n/a_{II})^2 - (\chi_m/b_I)^2} \left[\frac{2}{\pi} \frac{\chi_n b_I}{\chi_m a_{II}} J_1\left(\frac{\chi_n b_I}{a_{II}}\right) + \frac{\chi_n a_I}{a_{II}} J_1\left(\frac{\chi_n a_I}{a_{II}}\right) G'_1\left(\frac{\chi_m a_I}{b_I}\right)\right] \\ \quad \text{(TM coaxial waveguide mode and TM waveguide circular mode)} \\[1em] \left(\frac{\pi}{\eta_n^{TM}} C_n C_m\right) \frac{a_{II} b_I}{\chi_n \chi'_m} \left[-\frac{2}{\pi} \frac{1}{\chi'_m} J_1\left(\frac{\chi_n b_I}{a_{II}}\right) + J_1\left(\frac{\chi_n a_I}{a_{II}}\right) F_1\left(\frac{\chi'_m a_I}{b_I}\right)\right] \\ \quad \text{(TE coaxial waveguide mode and TM circular waveguide mode)} \\[1em] 0 \\ \quad \text{(TM coaxial waveguide mode and TE circular waveguide mode)} \end{cases} \tag{28}$$

The submatrices $[S_{11}]$, $[S_{12}]$, $[S_{21}]$, and $[S_{22}]$ are derived from $[P]$, $[Q]$, and $[R]$ by Eqs. (21) and (22):

$$[S_{11}] = \left[\sqrt{R}\right]\left([R] + [P]^T[P]\right)^{-1}\left([R] - [P]^T[P]\right)\left[\sqrt{R}\right]^{-1} \tag{29}$$

$$[S_{12}] = 2\left[\sqrt{R}\right]\left([R] + [P]^T[P]\right)[P]^T\left[\sqrt{Q}\right]^{-1} \tag{30}$$

$$[S_{21}] = 2\left[\sqrt{Q}\right]\left(\sqrt{Q} + [P][P]^T\right)[P]^T\left[\sqrt{R}\right]^{-1} \tag{31}$$

$$[S_{22}] = \left[\sqrt{Q}\right]\left([Q] + [P][P]^T\right)^{-1}\left([Q] - [P][P]^T\right)\left[\sqrt{Q}\right]^{-1} \tag{32}$$

When there are no dimension changes in the waveguide, which is then equivalent to a transmission line, the scattering matrix depends on the propagation constants of the waveguide modes in that straight section. To obtain the overall scattering matrix, the scattering matrices need to be cascaded. The procedure is described in detail in [1].

The above theory described the waveguide mode-matching method for coaxial-to-circular waveguide junctions. The same method was applied to circular-to-circular and coaxial-to-coaxial waveguide junctions (Figs. 3 and 4).

III. Computer Program Development

The geometrical configuration of the horn (flare angle, groove depth and width, and aperture size) is represented by a series of circular waveguides of different radii and lengths while the configuration of the disk-on-rod (diameter of the rod, diameter and thickness of the disk, disk spacing) is represented by a series of disks of various radii and lengths. These two data files are then combined and regenerated as a new data file containing the geometry of the disk-on-rod inside a horn. The new input data file includes the outer radius (horn), inner radius (disk-on-rod), and the length of the (either coaxial or circular) waveguide section. The inner radius is zero for circular waveguide sections. All the sections are circularly symmetric with respect to the center axis of the feedhorn. The number of modes in each section is chosen according to the ratio $M/N = (a_I - b_I)/(a_{II} - b_{II})$ in order to converge to the correct values.
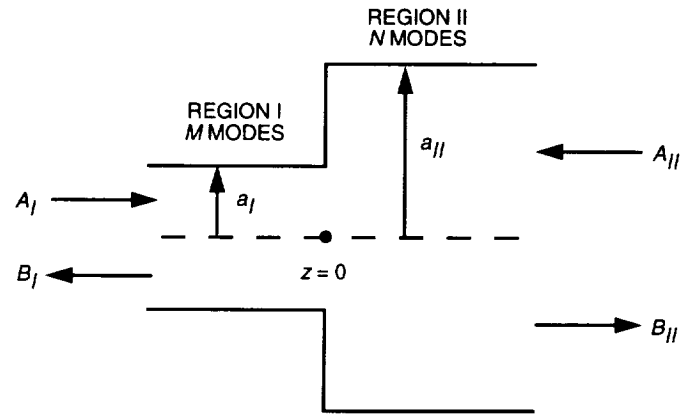
REGION II
N MODES

REGION I
M MODES

A_I

a_I

a_{II}

A_{II}

B_I

$z = 0$

B_{II}

Fig. 3. Circular waveguide junctions.

(a)

REGION I
M MODES

REGION II
N MODES

A_I

A_{II}

a_I

b_I

a_{II}

b_{II}
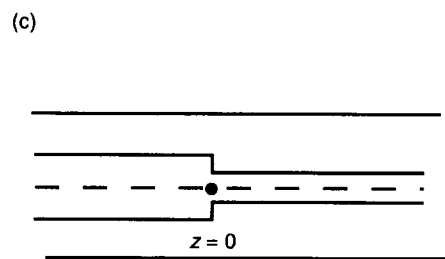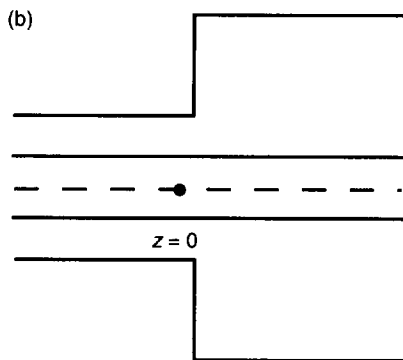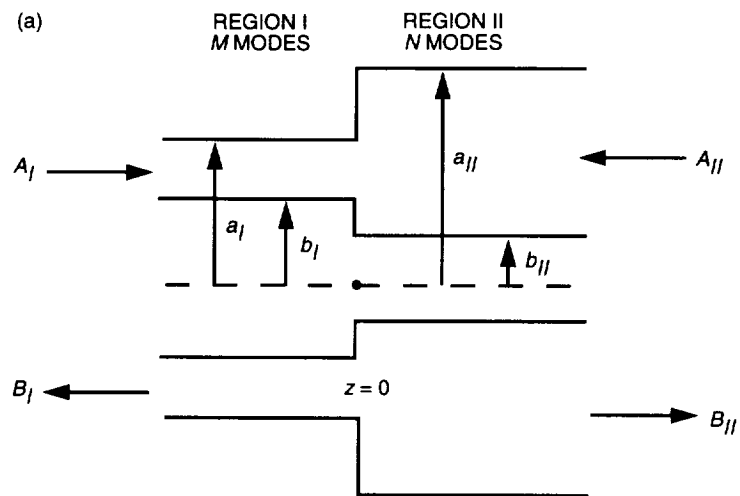
B_I

$z = 0$

B_{II}

(b)

$z = 0$

(c)

$z = 0$

Fig. 4. Coaxial waveguide junctions with a different (a) inner and outer
radius, (b) outer radius, and (c) inner radius.

The P, Q, and R are calculated [Eqs. (25)–(27)] according to the type and size of the waveguide junctions. The scattering matrix of each section is calculated and cascaded with the scattering matrix of previous sections until the scattering matrix of the whole horn is obtained.

The reflection matrix $[S_{11}]$ indicates the return loss of the horn. The radiation pattern can be computed by using the amplitude and phase of the transmitted circular waveguide modes ($[S_{12}]$) at the horn aperture [5]. Therefore, if the geometry of a feedhorn is available, both characteristics (radiation pattern and return loss) of the feedhorn are computed simply by inputting the geometrical dimensions to the computer program.

IV. Verification of the Computer Program

The program was first verified by comparing results with the existing circular waveguide program and coaxial waveguide program for appropriate junctions. Consistent results were achieved. Then an experiment was designed and performed in order to verify the scattering matrix of a circular-to-coaxial waveguide junction. The test piece is a WC137 circular waveguide with a circular aluminum rod suspended by two pieces of 0.0254 mm–thick kapton (Fig. 5). This structure includes a circular-to-coaxial and a coaxial-to-circular junction. The experiment was performed with rods of radii 7.62 and 10.16 mm and lengths of 63.5 and 76.2 mm. The amplitude and phase of the reflection (S_{11}) and transmission (S_{21}) coefficients were measured using a Hewlett Packard 8510C network analyzer. Good agreement between calculations and measurements was found in all the test cases. A test case of a rod of radius 7.62 mm and length 63.5 mm inside a WC137 circular waveguide of length 203.32 mm is shown in Figs. 6–9. The kapton in the waveguide was very thin in respect to the wavelength, so that it could be neglected in the computer modeling.

The L-/C-band dual-frequency horn, which includes a C-band disk-on-rod inside a C-band launcher and an L-band horn, was also used to check the computer codes (Fig. 10) [6]. By inputting the L-/C-band horn model in the program, the C-band and L-band radiation patterns were computed. Good agreement was shown between calculation and measurement at 5.01 GHz (C-band) and 1.668 GHz (L-band), respectively (Figs. 11–14) [7]. The slight asymmetry between the measured C-band E- and H-plane patterns was due to the C-band disk-on-rod becoming slightly off-centered during the trip to Goldstone, where the measurement was taken. All the results indicate that the software is reliable.
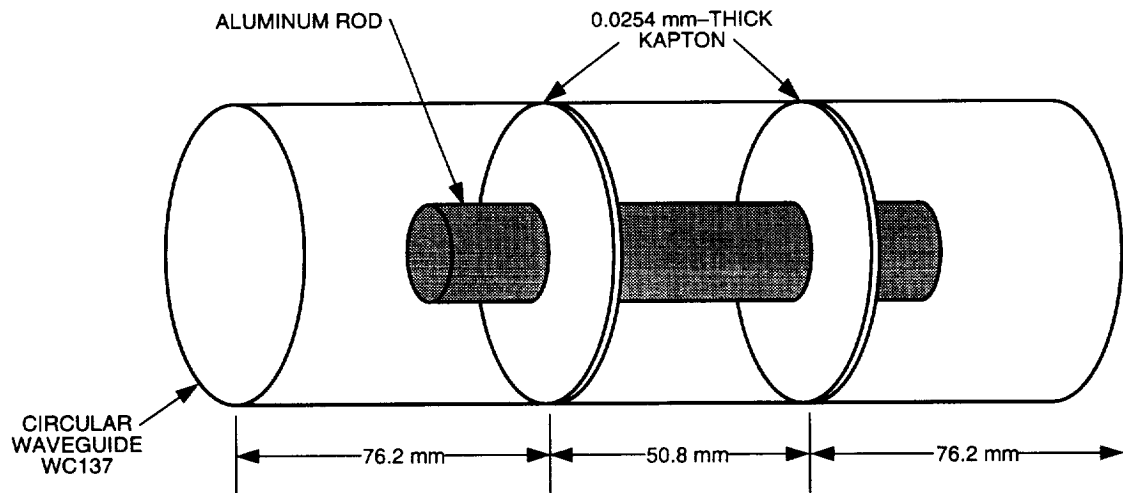

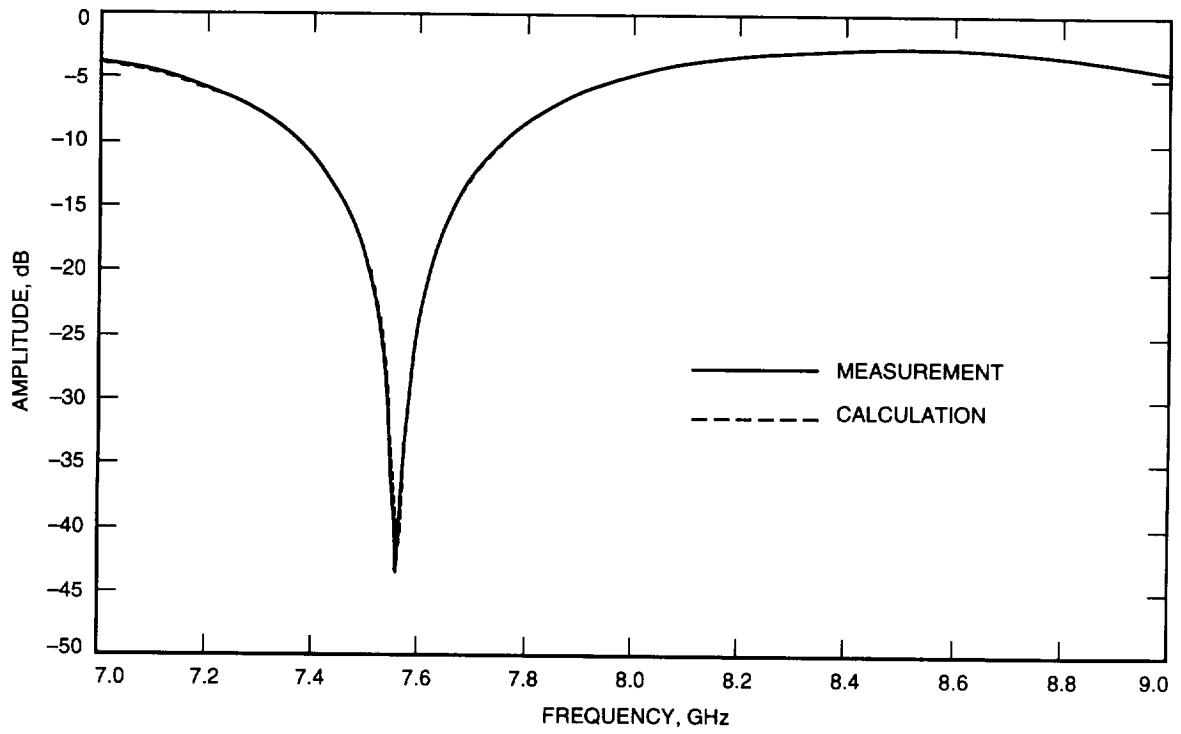Fig. 5. The test piece for the circular-to-coaxial and coaxial-to-circular junction experiment.

Fig. 6. Calculated and measured amplitude of S_{11} for a rod of radius 7.62 mm and length 63.5 mm inside a WC137 circular waveguide.
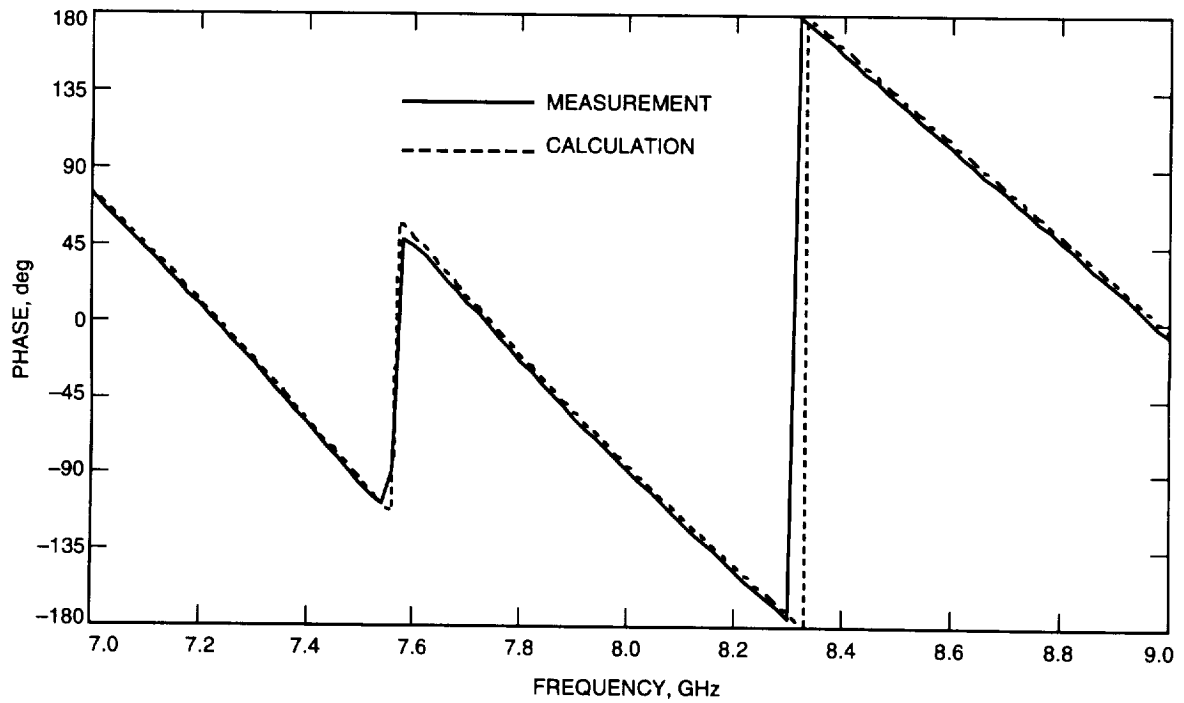

Fig. 7. Calculated and measured phase of S_{11} for a rod of radius 7.62 mm and length 63.5 mm inside a WC137 circular waveguide.
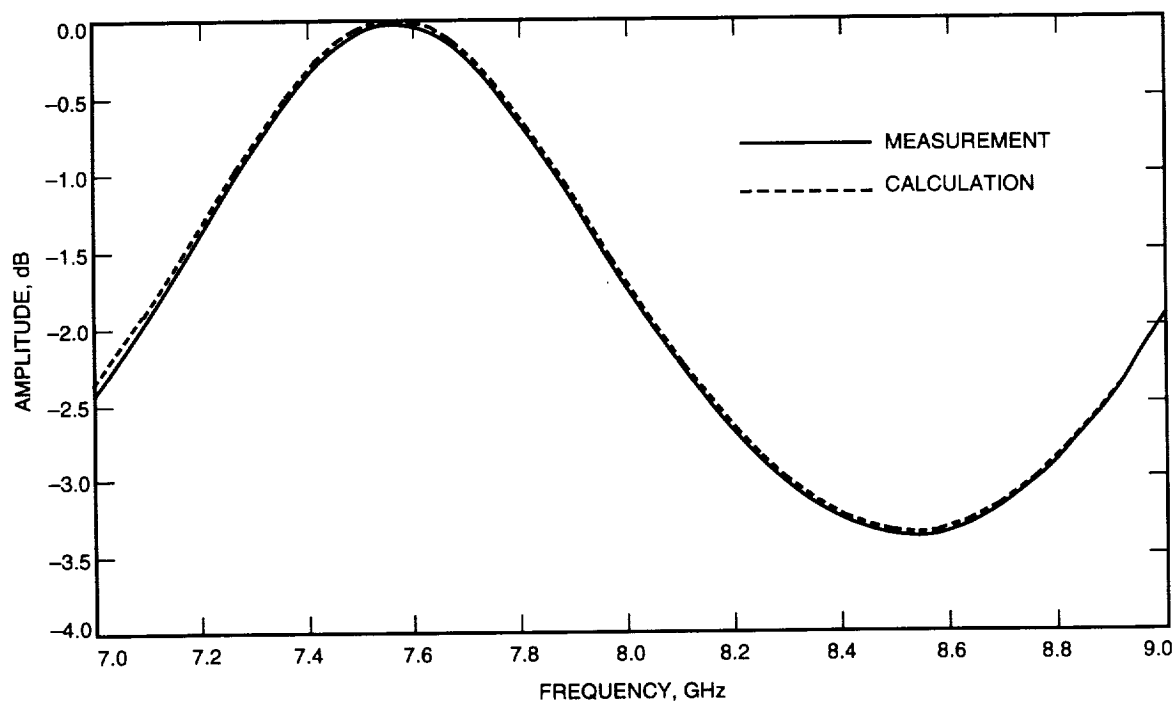
Fig. 8. Calculated and measured amplitude of S_{21} for a rod of radius 7.62 mm and length 63.5 mm inside a WC137 circular waveguide.
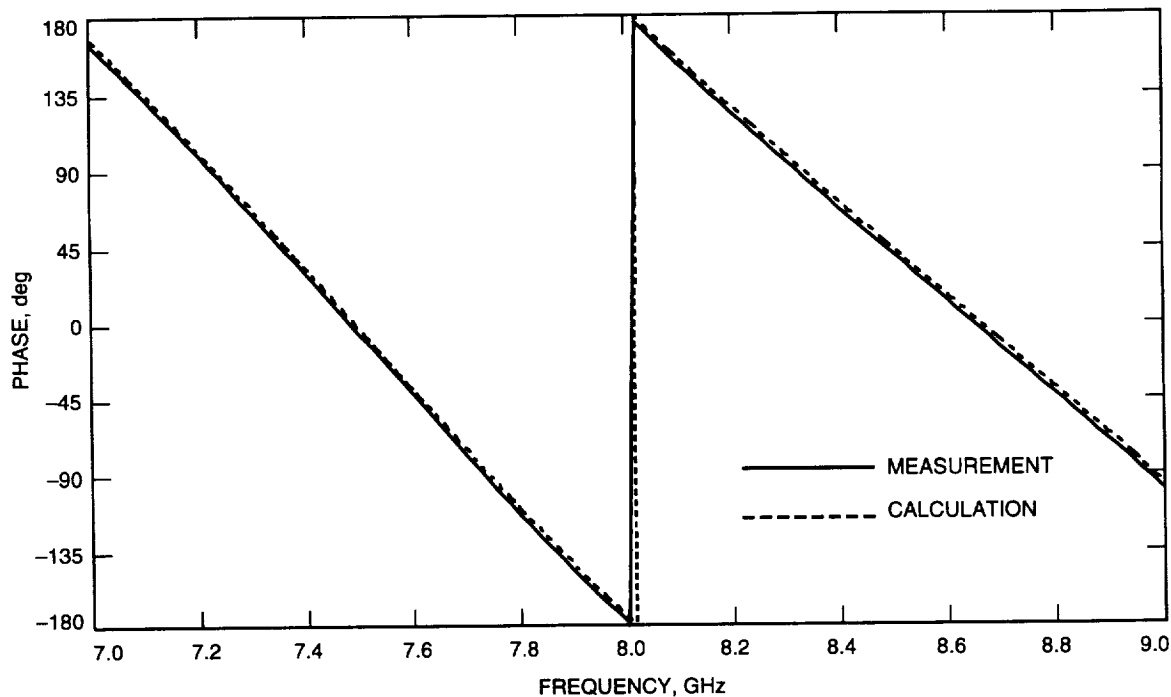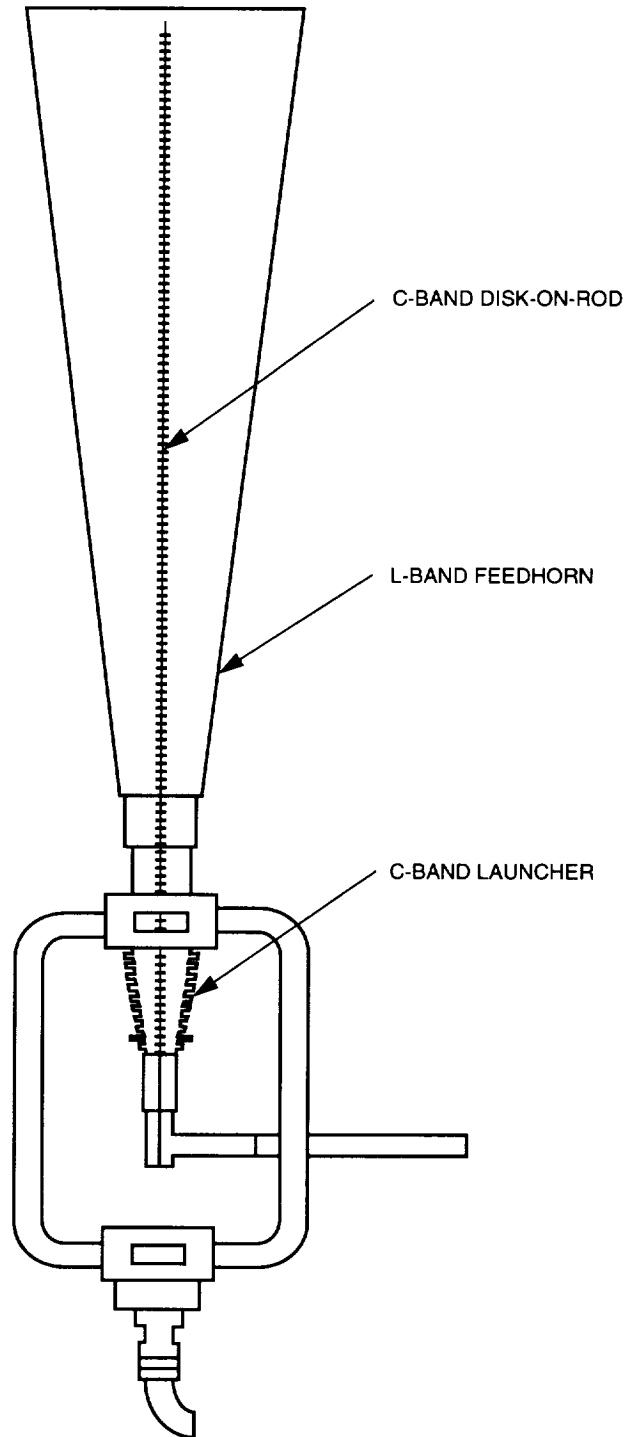

Fig. 9. Calculated and measured phase of S_{21} for a rod of radius 7.62 mm and length 63.5 mm inside a WC137 circular waveguide.

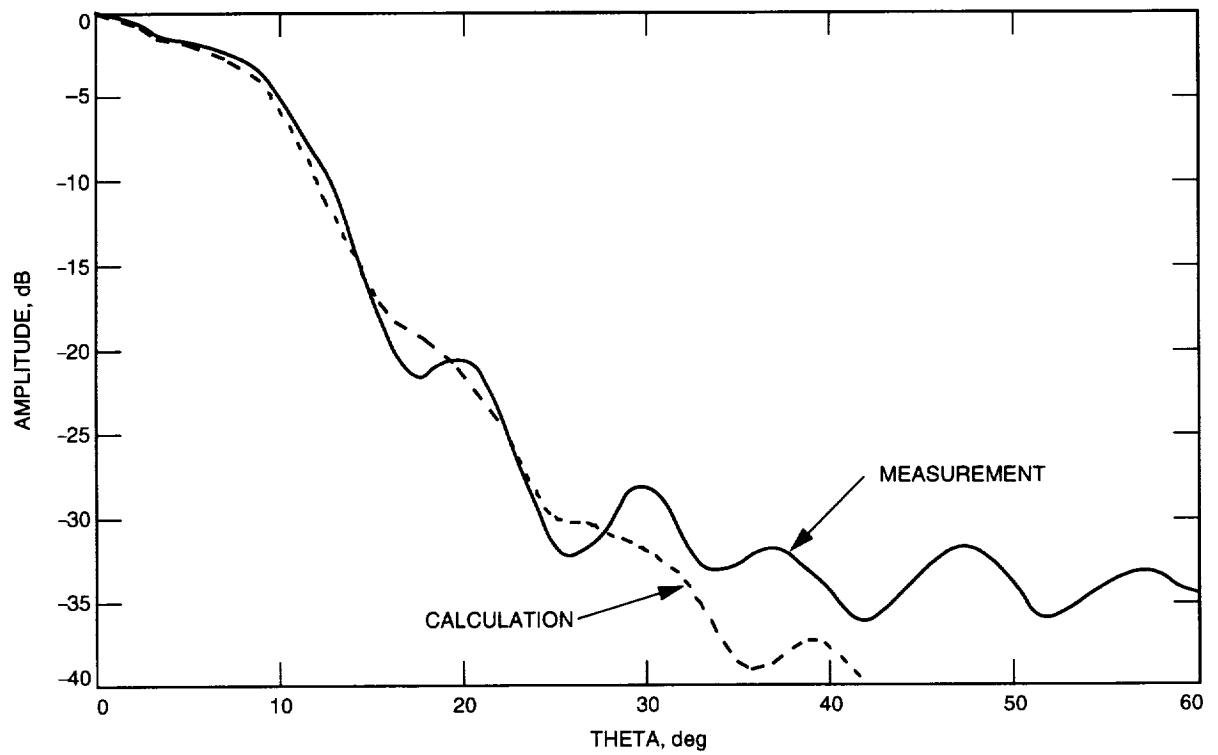Fig. 10. The L-/C-band dual-frequency feed system.

C-BAND DISK-ON-ROD

L-BAND FEEDHORN

C-BAND LAUNCHER

Fig. 11. Measured and calculated H-plane pattern for the L-/C-band dual-frequency horn at 5.01 GHz.
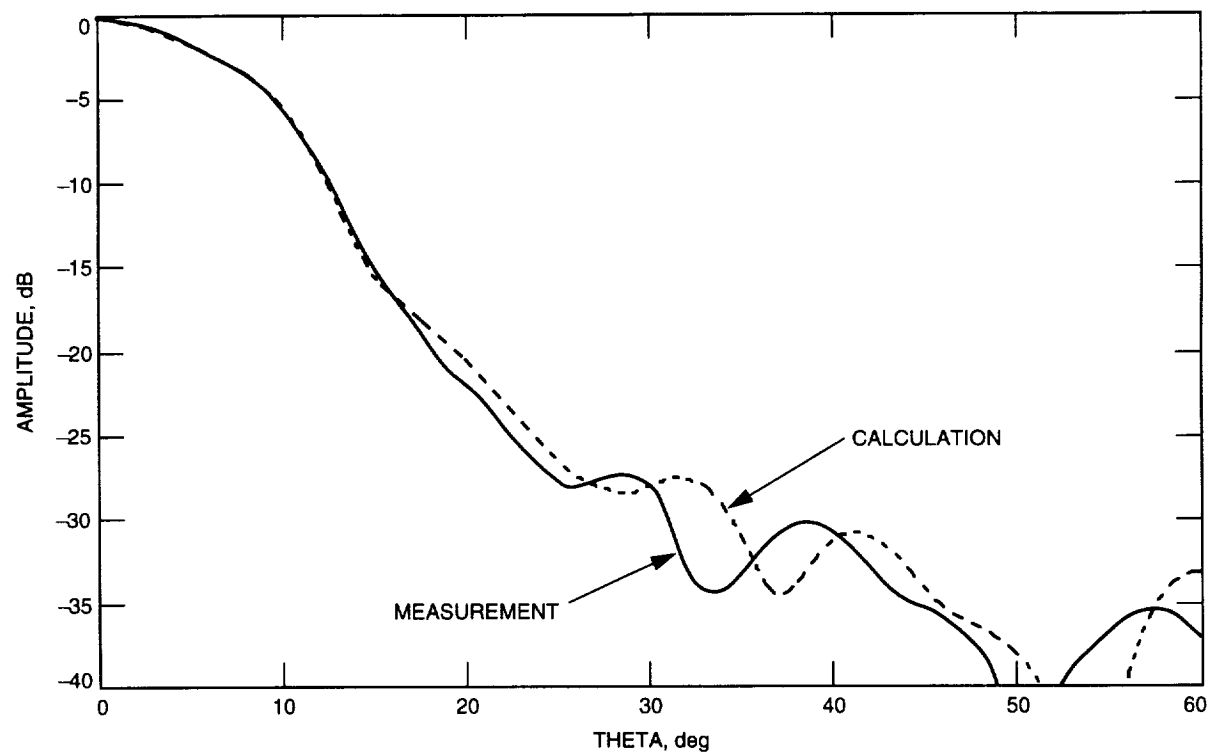

Fig. 12. Measured and calculated E-plane pattern for the L-/C-band dual-frequency horn at 5.01 GHz.
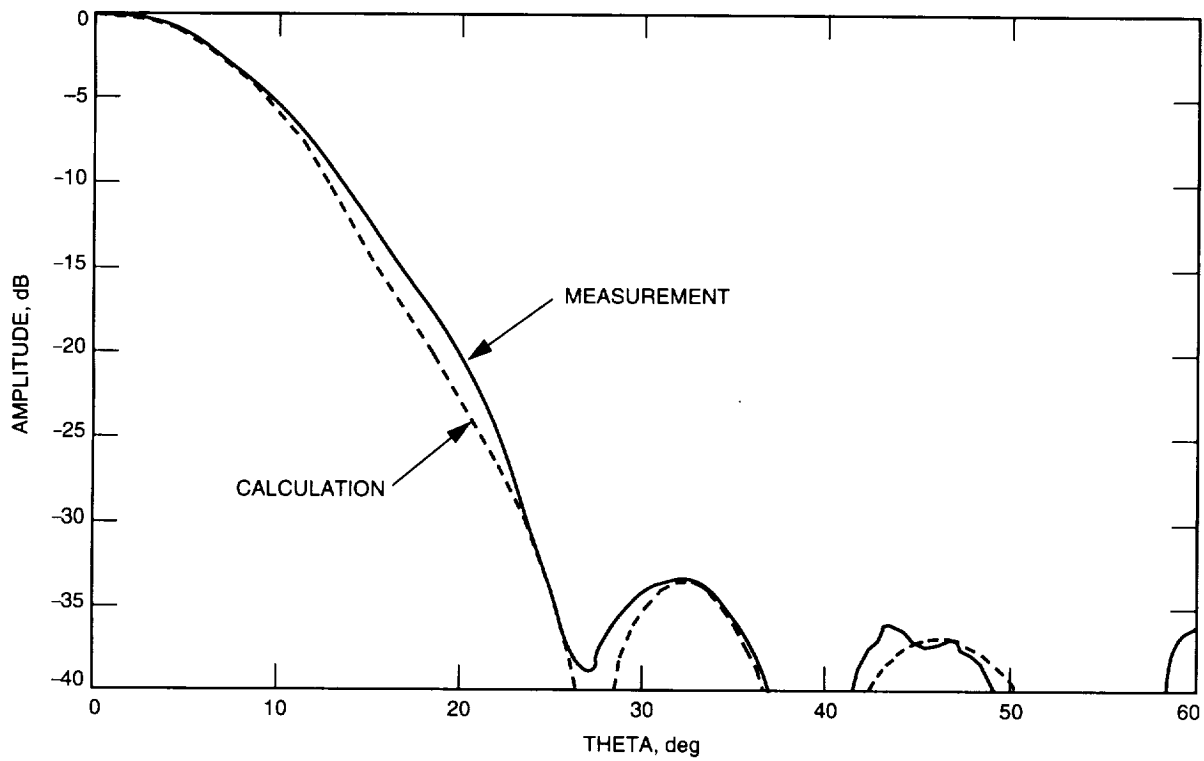
Fig. 13. Measured and calculated H-plane pattern for the L-/C-band dual-frequency horn at 1.7 GHz.
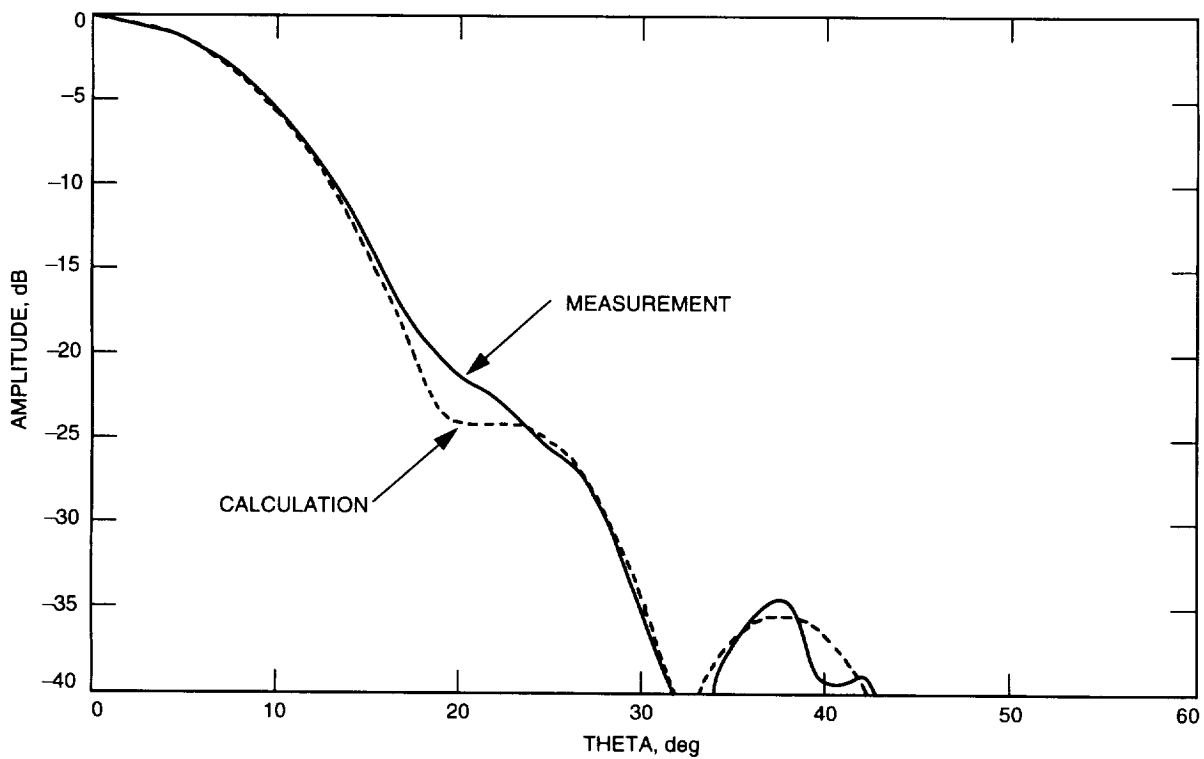

Fig. 14. Measured and calculated E-plane pattern for the L-/C-band dual-frequency horn at 1.7 GHz.

V. Conclusion

A disk-on-rod inside a horn was analyzed based on the mode-matching method. A computer program was developed to calculate the radiation pattern and the return loss of a horn by inputting the dimensions of the horn and the disk-on-rod. The computer program was verified by measurements and checked against other calculations. This software will be used to design an X-/Ka-band (8.45-GHz/33.7-GHz) dual-frequency horn for DSS 13.

Acknowledgment

References

[1] G. L. James, "Analysis and Design of TE_{11}-to-HE_{11} Corrugated Cylindrical Waveguide Mode Converters," *IEEE Transactions in Microwave Theory and Techniques*, vol. MTT-29, no. 10, pp. 1059–1066, October 1981.

[2] G. L. James and B. M. Thomas, "TE_{11}-to-HE_{11} Cylindrical Waveguide Mode Converters Using Ring-Loaded Slots," *IEEE Transactions in Microwave Theory and Techniques*, vol. MTT-30, no. 3, pp. 278–285, March 1982.

[3] D. J. Hoppe, "Modal Analysis Applied to Circular, Rectangular, and Coaxial Waveguides," *The Telecommunications and Data Acquisition Progress Report 42-95, July–September 1988*, Jet Propulsion Laboratory, Pasadena, California, pp. 89–96, November 15, 1988.

[4] N. Marcuvitz, *Waveguide Handbook*, United Kingdom: Peter Peregrinus Ltd., pp. 66–80, 1988.

[5] S. Silver, *Microwave Antenna Theory and Design*, New York: McGraw-Hill, pp. 336–337, 1949.

[6] P. H. Stanton and H. F. Reilly, Jr., "The L-/C-Band Feed Design for the DSS-14 70-Meter Antenna (Phobos Mission)," *The Telecommunications and Data Acquisition Progress Report 42-107, July–September 1991*, Jet Propulsion Laboratory, Pasadena, California, pp. 88–95, November 15,1991.

[7] M. S. Gatti, A. J. Freiley, and D. Girdner, "RF Performance Measurement of the DSS-14 70-Meter Antenna at C-Band/L-Band," *The Telecommunications and Data Acquisition Progress Report 42-96, October–December 1988*, Jet Propulsion Laboratory, Pasadena, California, pp. 117–125, February 15, 1989.